

Optimization stability in excited state-specific variational Monte Carlo

Leon Otis^a and Eric Neuscamman^{b,c}

^aDepartment of Physics, University of California Berkeley, CA 94720,USA; ^bDepartment of Chemistry, University of California Berkeley, CA 94720,USA; ^cChemical Sciences Division, Lawrence Berkeley National Laboratory, Berkeley, CA, 94720, USA

ARTICLE HISTORY

Compiled June 22, 2022

ABSTRACT

We investigate the issue of optimization stability in variance-based state-specific variational Monte Carlo, discussing the roles of the objective function, the complexity of wave function ansatz, the amount of sampling effort, and the choice of minimization algorithm. Using a small cyanine dye molecule as a test case, we systematically perform minimizations using variants of the linear method as both a standalone algorithm and in a hybrid combination with accelerated descent. We demonstrate that adaptive step control is crucial for maintaining the linear method's stability when optimizing complicated wave functions and that the hybrid method enjoys both greater stability and minimization performance. As a verification of variance minimization's practical utility, we report an excitation energy in the cyanine dye that is in good agreement with both benchmark quantum chemistry values and results obtained from state-averaged energy-based variational Monte Carlo.

KEYWORDS

Optimization; gradient descent; excited states; quantum Monte Carlo

1. Introduction

The challenges of wave function optimization have been a long-running thread in the development of Quantum Monte Carlo (QMC) methods. Ground state variational Monte Carlo (VMC) alone has seen significant evolution both in the optimization algorithms themselves[1–15] and the objective functions they are applied to.[7, 16–19] Early work on VMC optimization implemented steepest descent[20, 21] and Newton-Raphson[18, 22] for relatively small numbers of parameters in atoms and small molecules. As optimization algorithms, steepest descent and Newton-Raphson mark out two extremes in terms of derivative information and computational cost as purely first-order and fully second-order methods respectively. Subsequent methods, including approximate Newton,[3, 5] the linear method (LM),[1, 6, 7, 14] stochastic reconfiguration,[4, 8, 9] and accelerated descent (AD),[10–13] can be broadly viewed as pursuing a balance between the advantages of second-order derivative information against the cost of obtaining it. This profusion of different techniques, spread among many research groups, has motivated recent efforts to systematically compare their

performance and identify effective combinations of them.[15]

The need to achieve robust VMC optimization has also surfaced more recently in the context of excited state VMC. For this frontier in VMC, both energy-based state-averaged and variance-based state-specific objective functions have been developed for describing excited states. State-averaged energy minimization has been successful in many applications,[23–29] while the state-specific approach[30–35] offers advantages in cases where the appropriate orbital shapes for the relevant states differ significantly. These considerations are also present in deterministic methods such as CASPT2[36–38] and are especially important when studying charge transfer states[35, 39–41] and core excitations.[33]

Methodological advancements have steadily occurred in recent years for both state-averaged and state-specific VMC. Many innovations can be readily adopted within both frameworks such as improvements in ansatz design with selected CI (sCI) expansions[29, 42, 43] and new optimization algorithms.[15, 34, 35, 44] In addition, multiple protocols[29, 33, 35, 43, 45] have been developed to ensure balanced treatments of different states, a prerequisite for obtaining accurate excitation energies. The progress on all these fronts has helped advance excited-state VMC from initial applications[3, 16, 30, 46] with small molecules and simple wave functions to much wider use on larger systems with more sophisticated ansatzes.[29, 35]

Given the promise of VMC as a reliable tool for excited states, recent research[28] raising concerns about the stability of variance minimization in VMC merits close attention. In a small cyanine dye molecule, Filippi and coworkers found failures of variance minimization to converge to the correct excited state even for high quality wave function ansatzes. In some cases, a lowering of the variance was accompanied by a substantial rise in the energy as the optimization moved to some undesired state. The authors attributed this behavior to the shape of the variance optimization surface, with the optimization finding “little or no barrier to escape from a local minimum or local plateau, eventually converging to a lower-variance state instead of the target state.”[28] This hypothesis would imply that the same behavior might be observed in other excited state applications of variance minimization, posing a significant obstacle to successful excitation energy predictions. In the present study, we investigate instabilities in variance optimization in order to better understand where they come from, whether a pathological variance surface shape is the best explanation for these instabilities, and how they may be addressed.

The issue of stability in VMC optimization is multi-faceted, with technical considerations about the choice of objective function, the particular optimization algorithm used, the level of sampling effort, and the quality of wave function ansatz each playing a role. Deficiencies in any of these areas could potentially lead to failures of optimization, and no approach to optimization is likely to be successful in absolutely all circumstances. However, the relevant question for VMC practitioners is whether these instances of optimization failure pose an insurmountable barrier in practice or whether they can be remedied with certain choices in methodological protocol.

At a broad conceptual level, the objective function being minimized and the particular wave function ansatz set the difficulty of a VMC optimization. Compared to the energy, the variance landscape in parameter space is more difficult to resolve at a given level of sampling effort and estimates of its derivatives may also be more uncertain.[28, 47, 48] While increasing the amount of sampling enables systematic improvement of these estimates, the availability of computational resources inevitably places some practical upper limit. The shape of the landscape will also vary with the particular wave function form that is chosen. An isolated minimum of zero variance

is guaranteed for any non-degenerate exact eigenstate and some minimum can be expected to form when a wave function is systematically built up to this limit, as in a Slater determinant expansion. However, the depth and shape of the minimum are difficult to characterize and the ansatz parameters are unlikely to be set to the optimal values initially in practice. As a result, the particular optimization algorithms chosen to navigate the parameter landscape must be highly robust to noisy gradients and capable of handling increasing numbers of parameters. We shall see that different types of algorithms with varying levels of step control can be more or less prone to take poor steps when the number of parameters is large and statistical noise affects their updates. Indeed, poor steps due to poor step control appear to be a leading factor behind optimization instabilities, making more robust step control highly effective.

To further elucidate the issue of optimization stability in VMC, we conduct systematic investigations of the LM in the case of the excited state of the cyanine dye molecule CN5 that has previously shown instabilities. We focus on identifying circumstances where variance minimization with the LM fails and what can be done to resolve these failures. Beyond technical choices in operating the LM, we also consider the stability advantages offered by a hybrid combination of the LM’s blocked variant and AD, particularly those rooted in adaptive step control. As we will see, multiple optimization choices play a role in optimization effectiveness, but the key determiner of stability appears to be adaptive step control, analogous to using an adaptive trust radius. In particular, we do not find any indications that variance optimization instabilities arise from pathologies in the objective function surface. If this were the case, all optimization methods regardless of adaptive step control would eventually show instabilities as well. As our data below demonstrates, even cases previously reported as unstable become stable when sufficiently robust adaptive step control is applied.

2. Theory

2.1. Objective Functions in VMC

Analysis of optimization stability within VMC begins with consideration of the objective or target function being minimized. A variety of choices have been employed by VMC practitioners, for both ground and excited state studies, with the most common choices being the energy or the variance of the energy for the system at hand.

$$E(\vec{\mathbf{p}}) = \frac{\int \Psi_T^2(\vec{\mathbf{p}}) E_L(\vec{\mathbf{p}}) d\vec{\mathbf{R}}}{\int \Psi_T^2(\vec{\mathbf{p}}) d\vec{\mathbf{R}}} \quad (1)$$

$$\sigma_E^2(\vec{\mathbf{p}}) = \frac{\int \Psi_T^2(\vec{\mathbf{p}}) (E_L(\vec{\mathbf{p}}) - E(\vec{\mathbf{p}}))^2 d\vec{\mathbf{R}}}{\int \Psi_T^2(\vec{\mathbf{p}}) d\vec{\mathbf{R}}} \quad (2)$$

In the above definitions, $E_L = \frac{H\Psi(\mathbf{R})}{\Psi(\mathbf{R})}$ is the local energy. Historically, numerical instabilities in early VMC energy minimizations motivated the use of variance minimization,[16, 17, 19] but later algorithmic improvements, particularly the development of the linear method,[7] have swung the pendulum back to energy minimization as the main approach for ground state studies. The choice of objective function is less

settled for the study of excited states and both energy-based[23–29] and variance-based[16, 30–34] objective functions have been employed in this context.

$$\Omega(\Psi) = \frac{\langle \Psi | (\omega - H) | \Psi \rangle}{\langle \Psi | (\omega - H)^2 | \Psi \rangle} \quad (3)$$

$$W(\Psi) = \langle \Psi | (\omega - H)^2 | \Psi \rangle \quad (4)$$

$$E^{SA} = \sum_I w_I \frac{\langle \Psi^I | H | \Psi^I \rangle}{\langle \Psi^I | \Psi^I \rangle} \quad (5)$$

The functions Ω and W both use an input energy parameter ω to ensure targeting of a desired excited state. While ω is held fixed when performing an update to wave function parameters, it must ultimately be adjusted to transform Ω and W into the variance σ^2 to obtain size-consistent results.[31] For Ω , the value ω must eventually be set to the difference of the energy and standard deviation, $E - \sigma$, while for W , ω must eventually be set to the energy E . There are multiple strategies for varying ω , either allowing it to float based on the values of E and σ over the course of a single VMC optimization, or performing multiple VMC optimizations at fixed ω and changing the value after each one until self-consistency is achieved. From the standpoint of optimization stability, allowing the value of ω to vary is one potential source of instability as stochastic uncertainties in the value assigned to ω could possibly lead to the targeting of a different state, and so we investigate this possibility below. We also note that there are various options in the details of varying ω , such as allowing it to float only after a period of interpolation from its initial value[31] or controlling its value through a running average.

The effectiveness of stochastic estimation of different quantities is another factor in the stability implications of the choice of objective function. Sampling from the commonly chosen distribution $\rho(\mathbf{R}) = \frac{\Psi(\mathbf{R})^2}{\int d\mathbf{R} \Psi(\mathbf{R})^2}$ has a zero variance property[49] when Ψ is an exact eigenstate, but the use of approximate Ψ in practice leads to an infinite variance problem for the estimation of the variance itself as well as target function derivatives.[47, 48] While the infinite variance of the variance makes optimization of variance-based target functions more difficult, multiples approaches for mitigating the issue have been developed, including the use of other importance sampling functions,[32, 34, 45, 47, 48, 50] modifications to estimators,[49, 51, 52], and regularization schemes.[53, 54] We employ an importance sampling function that we have successfully used in the minimization of the Ω objective function in other work.[34, 35]

$$|\Phi|^2 = |\Psi|^2 + c_1 \sum_i |\Psi^i|^2 + c_2 \sum_j |\Psi^j|^2 + c_3 \sum_k |\Psi^k|^2 \quad (6)$$

In $|\Phi|^2$, the coefficients c_1, c_2, c_3 weight the sums of squares of wave function parameter derivatives for Jastrow, CI, and orbital parameters respectively and we set $(c_1, c_2, c_3) = (0.0, 0.0001, 0.0)$ throughout our results.

2.2. Parameter Optimization Algorithms

A variety of algorithms have been developed for performing parameter optimization in the context of VMC. Some of the most notable ones include the Newton method,[2, 3, 5, 28, 55] the linear method (LM),[1, 6, 7, 14, 55] stochastic reconfiguration, (SR)[8] and accelerated descent (AD) approaches.[10–13, 15] We focus our discussion on only the aspects of the LM and AD that are most relevant for optimization stability. Further details on these methods can be found in the literature.[1, 6, 7, 10–13, 15, 44, 55]

The LM relies on a first order Taylor expansion of the trial wave function and in the case of minimizing Ω leads to a generalized eigenvalue problem

$$(\omega - \mathbf{H}) \mathbf{c} = \lambda (\omega - \mathbf{H})^2 \mathbf{c} \quad (7)$$

with matrix elements of the form

$$\langle \Psi_i | \omega - H | \Psi_j \rangle \quad (8)$$

and

$$\langle \Psi_i | (\omega - H)^2 | \Psi_j \rangle. \quad (9)$$

where Ψ_i and Ψ_j are wave function derivatives with respect to variational parameters. The LM requires stochastic estimates of these matrix elements to compute an update \mathbf{c} to the wave function parameters. The size of the LM matrices will grow as the square of the number of parameters. For a fixed number of statistical samples, increasing the number of parameters can increase the uncertainty in the LM’s parameter update steps, which in turn increases the risk of optimization failure.

An example illustrating this issue is given in Figure 1, which shows the spreads of proposed LM updates on the same Jastrow parameter when increasing total numbers of parameters are included at a fixed statistical sample size. As more CI parameters are added, the statistical spread of the updates to this Jastrow parameter increases by an order of magnitude. What is going on here is that the LM’s eigenproblem effectively amplifies and couples the noise in the updates for individual parameters. If this were not the case, the spread in the Jastrow update would remain constant regardless of how many parameters were included. Given that the degree of nonlinearity present in a diagonalization grows with matrix dimension, it is not entirely surprising that diagonalizations of larger and larger sets of statistically uncertain matrix elements lead to increased uncertainty in the proposed parameter updates. For larger numbers of parameters, naive acceptance of these increasingly uncertain LM updates could lead to instabilities in optimization, which strongly suggests that step control methods that work to reduce this uncertainty and that adapt their behavior based on the degree of uncertainty will be valuable.

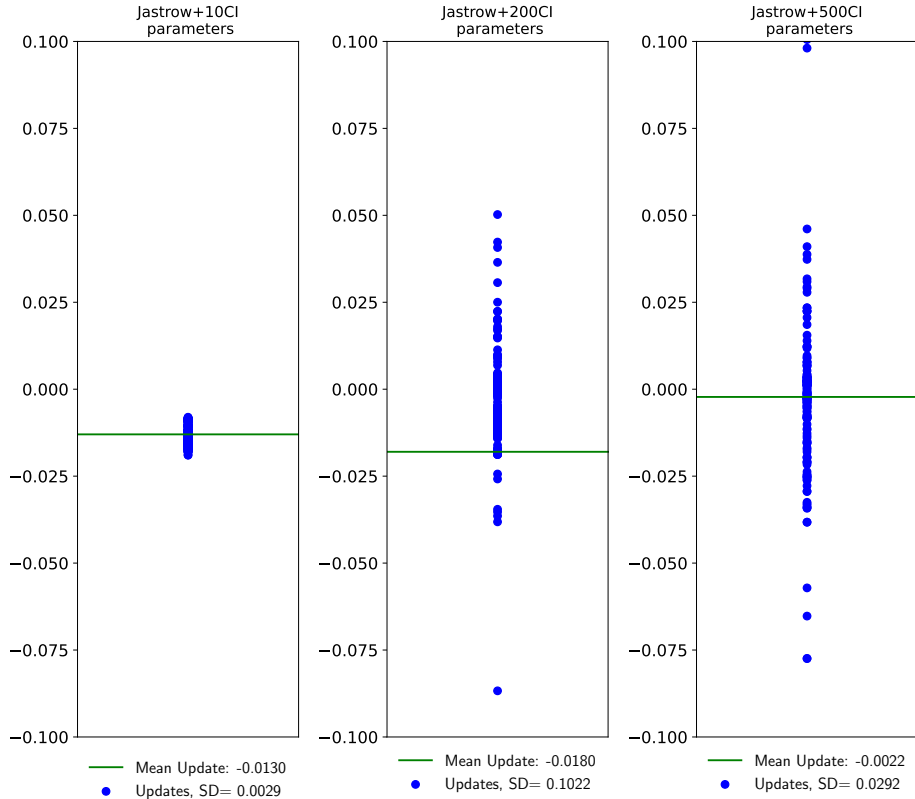


Figure 1. Proposed LM updates to a Jastrow spline parameter for varying total numbers of parameters. Each panel was produced with 200 proposed updates from independent LM runs on an excited state wave function in CN5. The same scale has been used in each panel, which leaves off some larger outliers in the 200 and 500 determinant cases. From left to right, the total numbers of wave function parameters for the different cases are 150, 340, and 640. 100,000 samples were used to generate the LM matrices for each update.

A number of technical modifications to the basic LM algorithm can reduce, though not eliminate, this problem. Shift values can be added to the LM Hamiltonian matrix to prevent overly large parameter changes, similar to the use of trust radius schemes in Newton-Raphson.[15, 56] Two different types of shifts, defined in equations 10 through 14, can help address distinct problems in the LM optimization. The diagonal shift c_I helps stabilize the LM by effectively adding an energy penalty to parameter changes to the current wave function.[7] While this shift reduces the effective step size of the LM, it also changes the direction of the LM updates by rotating them to the steepest descent direction in the limit of an infinite shift.[6] Figure 2 demonstrates the effect of a large diagonal shift in controlling the noise in parameter updates. The spread of proposed updates for the Jastrow parameter is very small and also remains constant across the different total numbers of parameters, which is the behavior expected in steepest descent. It is important to emphasize that the step damping parameter used in the previous CN5 study[28] does not have this effect. It only scales the step after the step has been evaluated, meaning that when using it without any other step control method, the phenomenon of step uncertainty increasing with parameter number will still be present.

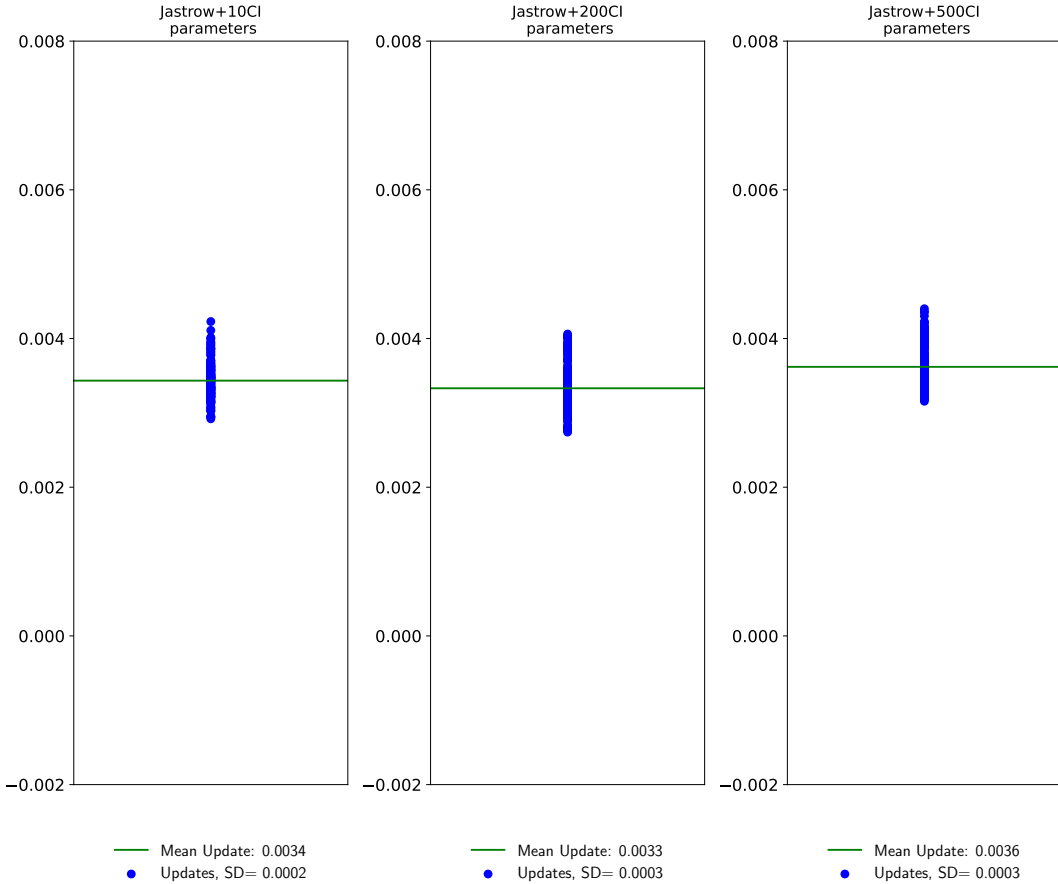


Figure 2. Proposed LM updates to a Jastrow spline parameter with a diagonal shift of 100 for varying total numbers of parameters. Each panel shows 200 proposed updates from independent LM runs with an excited state wave function in CN5. 100,000 samples were used to generate the LM matrices for each update.

While the diagonal shift prevents excessive changes in parameters with large derivatives, assigning it a large enough value for this task may turn off the optimization of parameters with smaller, but still significant gradients. To avoid this scenario, the $c_S \mathbf{B}$ term helps retain flexibility in other parameter directions with smaller derivatives. The overlap shift c_S imposes an energy penalty based on the norm of parameter directions orthogonal to the current wave function so that steps in the directions of small derivatives are penalized less heavily and meaningful changes in them can still occur. In practice, the matrix \mathbf{B} does not need to be constructed explicitly, as the LM generalized eigenvalue problem can be solved by Krylov iteration.[14, 56]

$$\mathbf{H} \rightarrow \mathbf{H} + c_I \mathbf{A} + c_S \mathbf{B} \quad (10)$$

$$A_{ij} = \delta_{ij}(1 - \delta_{i0}) \quad (11)$$

$$\mathbf{B} = (\mathbf{Q}^T)^{-1} \mathbf{T} \mathbf{Q}^{-1} \quad (12)$$

$$Q_{ij} = \delta_{ij} - \delta_{i0}(1 - \delta_{j0})S_{0j} \quad (13)$$

$$T_{ij} = (1 - \delta_{i0}\delta_{j0})[\mathbf{Q}^T \mathbf{S} \mathbf{Q}]_{ij} \quad (14)$$

In our own implementation of the linear method, the use of shifts is enhanced in combination with an adaptive scheme[6, 7, 55] where three sets of shift values are used to determine parameter updates, and a correlated sampling procedure either selects the candidate update expected to reduce the objective function the most, or rejects all the possible updates and raises the shifts on the next LM iteration for more cautious steps. This allows the step control to account in at least a limited way for the amount of statistical uncertainty present in a given stage of the optimization. Despite this ability to reject poor steps and the stability benefits it offers, we will show in our results that this approach to the LM can still fail to lower the objective function effectively in some circumstances.

A more substantial modification to the LM is to divide the parameters into blocks and solve a set of smaller eigenvalue problems to produce the parameter update.[44] The blocked LM algorithm consists of two phases. First, an LM-style diagonalization is performed for each of the N_b blocks of parameters and the N_k lowest eigenvectors are retained from each block. In the second phase, the full set of $N_b N_k$ eigenvectors plus N_o other parameter directions (either from previous blocked LM iterations or descent, in the case of the hybrid method) form the space for a final LM diagonalization that gives the overall update. This approach provides the blocked LM with a lower memory footprint compared to the standard LM, but reduces the flexibility of the directions it can explore in parameter space. By working with smaller matrices, however, the blocked LM reduces the degree of nonlinear coupling in its equations and thus directly addresses the issue shown in Figure 1. It therefore has the potential to provide more reliable update steps. However, in the limit of more variational parameters with insufficient sampling effort, the blocked LM will share the same vulnerabilities as the standard LM.

AD methods are a class of pseudo-first-order optimization algorithms that use only the gradient of the target function, retaining some memory of gradients from previous iterations in order to converge more quickly than steepest descent. Many different flavors of AD have been widely used in the machine learning community and a number of them have been applied in the context of VMC.[10–13, 15] Below, we give the defining equations for a combination of RMSprop and Nesterov momentum as used in a number of VMC studies[10, 15, 34, 35] and which we use here in the hybrid method.

$$p_i^{k+1} = (1 - \gamma_k e^{-\frac{1}{d}(k-1)})q_i^{k+1} - \gamma_k e^{-\frac{1}{d}(k-1)}q_i^k \quad (15)$$

$$q_i^{k+1} = p_i^k - \tau_k \frac{\partial \Omega(\mathbf{p})}{\partial p_i} \quad (16)$$

$$\lambda_0 = 0 \quad \lambda_k = \frac{1}{2} + \frac{1}{2} \sqrt{1 + 4\lambda_{k-1}^2} \quad \gamma_k = \frac{1 - \lambda_k}{\lambda_{k+1}} \quad (17)$$

$$\tau_k = \frac{\eta}{\sqrt{E[(\frac{\partial \Omega}{\partial p_i})^2]^{(k)} + \epsilon}} \quad (18)$$

$$E[(\partial \Omega)^2]^{(k)} = \rho E \left[\left(\frac{\partial \Omega}{\partial p_i} \right)^2 \right]^{(k-1)} + (1 - \rho) \left(\frac{\partial \Omega}{\partial p_i} \right)^2 \quad (19)$$

The recurrence relations defined in equations 15 through 17 define the momentum in this algorithm. Obtaining the updated parameter p_i^{k+1} depends on the values of the target function gradient $\frac{\partial \Omega(\mathbf{p})}{\partial p_i}$ from both the present and previous iterations, which accelerates the convergence compared to steepest descent. Equations 18 and 19 define the RMSprop adaptive modification of the step size τ_k , which is parameter-specific.

From a stability perspective, AD approaches offer a number of advantages compared to the LM. The relevant equations are far more linear than the LM's generalized eigenvalue problem, which reduces the dangers of step bias and uncertainty from nonlinear combinations of stochastic quantities. In practice, VMC optimization with AD can be conducted with a significantly lower per-iteration sampling effort than the LM without creating instabilities. While an individual AD step may be poor and raise the objective function, modest step sizes ensure that the change to the wave function is small, and typical AD optimizations use many hundreds or thousands of iterations to successfully minimize the objective function. However, these stabilizing features of AD also leave it slower to converge to the minimum than the LM.[15] This weakness has motivated the development of a hybrid approach that alternates between sections of AD and blocked LM optimization, in order to allow the blocked LM to more swiftly move parameters to their optimal values.[15, 34, 35]

2.3. Wave Functions

Another key aspect of VMC stability is the choice of wave function, which shapes the target function landscape and thus the difficulty of the optimization problem. With the exact wave function and an infinite sample size, variance minima will exist for all the non-degenerate Hamiltonian eigenstates.[16] For approximate ansatzes and finite sampling effort, the minima may become shallow enough that some optimizers fail to target and converge to them or they may not exist at all. Therefore, as a practical matter, being able to systematically improve the wave function and the amount of sampling may make the difference between success and failure for a given optimization algorithm. We have provided a recent example of this by applying the LM to simple wave functions in CN5, where adding a 3-body Jastrow factor and increasing sampling eliminated instabilities.[34]

In this work, we consider more complex wave functions in CN5, all of the Multi-Slater Jastrow (MSJ) form shown below. The Slater determinant expansion ψ_{MS} can be obtained from various active space calculations of different sizes, with larger spaces potentially solved by sCI, producing longer and more accurate expansions.

$$\Psi = \psi_{MS}\psi_J \quad (20)$$

$$\psi_{MS} = \sum_{i=0}^{N_D} c_i D_i \quad (21)$$

$$\psi_J = \exp \left\{ \sum_i \sum_j \chi_k(|r_i - R_j|) + \sum_k \sum_{l>k} u_{kl}(|r_k - r_l|) \right\} \quad (22)$$

Throughout our results, we employ and optimize one- and two-body Jastrow factors, which are constructed with splines for the functions χ_k and u_{kl} .^[56] For our stability analysis, we also optimize the orbitals of our Slater expansions, benefiting from recent methodological improvements with the table method.^[57, 58] However, as we show in our results, orbital optimization can still be challenging for the LM, and we also consider VMC optimization with the orbitals left at shapes obtained from a recent state-specific CASSCF approach.^[38, 59, 60] This approach of combining state-specific quantum chemistry with VMC has recently been shown to provide accurate excitation energies across a range of different types of excited states^[35] and we provide another example of this here for the excited state in CN5. However, the key thrust of the present study is optimization stability, and so in many of our results we will be optimizing orbitals within VMC to test stability in that context.

3. Results

3.1. Computational Details

We perform all VMC optimizations in a development version of QMCPACK.^[56, 61] Our molecular geometry is identical to one recently used by Filippi and coworkers^[28, 62] and we repeat the coordinates in the appendix for convenience. Basis set and pseudopotential choices are specified below for the particular wave function cases we consider. For generating our wave functions, we have performed CASSCF calculations in Molpro^[63] and PySCF,^[64] as well as sCI calculations in Dice.^[65, 66] Our one- and two-body Jastrow factor splines each consist of 10 coefficients defining the function within a cutoff distance of 10 bohr.

3.2. Excitation Energies from Variance Minimization

We begin by simply checking the ability of variance-based excited state VMC to obtain accurate excitation energies with the hybrid method. For this test, we follow the same methodology that has recently been applied on a broader set of excited states.^[35] We

use a cc-pVTZ basis set with pseudopotentials[67] and obtained state-specific CASSCF orbitals in a (6e,5o) space. We then generate Slater determinants from heatbath CI in a (28e,40o) space of these orbitals. The orbitals are left at their state-specific CASSCF shapes and we optimized only Jastrow parameters and CI coefficients in VMC with the hybrid method, using a recent parameter selection scheme[35] to optimize only parameters with significant derivatives within the blocked LM. For the blocked LM portions, we divided those parameters into 5 blocks and retained 30 parameter directions per block along with 5 directions from AD for the second phase of the blocked LM algorithm. No stability issues were observed in these optimizations. Our VMC wave functions used 500 determinants for the ground state and 1000 for the excited state. A recently introduced variance matching extrapolation procedure[35] is used to ensure a balanced treatment of the ground and excited states.

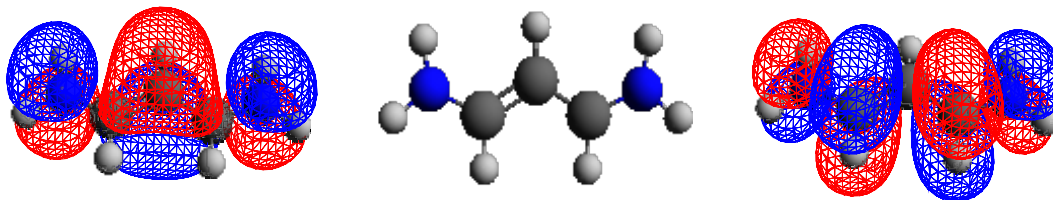


Figure 3. Structure (center) for CN5: $C_3H_3(NH_2)_2^+$. Hole (left) and particle (right) orbitals for the CN5 excited state.

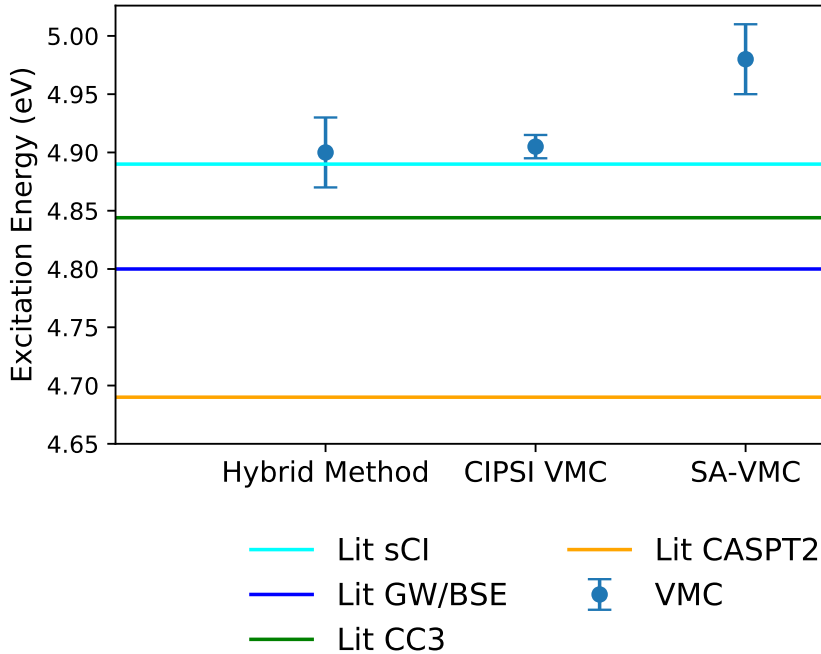


Figure 4. Excitation energy in CN5 using the hybrid method to minimize the Ω target function. Reference values for SA-VMC and CIPSI VMC,[28] CC3,[28] CASPT2,[25, 62] GW/BSE,[62] and sCI[68] are taken from the literature. For comparison, the basis sets used in the literature results were aug-cc-pVTZ for CC3 and GW/BSE, aug-cc-pVDZ for sCI, ANO-L-VTZP for CASPT2, and a double- ζ basis set minimally augmented with s and p diffuse functions on heavy atoms for SA-VMC and CIPSI VMC.

Table 1. Excitation energies for CN5 for state-specific VMC and literature results.[25, 28, 62, 68] Stochastic uncertainties on the last digit are given in parentheses. The values for SA-VMC and CIPSI were obtained from VMC energy minimizations using wave functions from a (14e, 13o) CAS and balanced CIPSI expansions respectively.[28]

Method	Excitation Energy (eV)
Hybrid Method VMC	4.90(3)
SA-VMC	4.98(3)
CIPSI VMC	4.91(1)
CASPT2	4.69
GW/BSE	4.80
CC3	4.84
sCI	4.89

As shown in Figure 4 and Table 1, we obtain a highly accurate excitation energy for this state in CN5 for our variance-based methodology. Our result is with 0.1 eV of literature results from sCI[68] and CC3[28] and statistically indistinguishable from a VMC result from Filippi and coworkers based on minimizing the state-averaged energy.[28] Thus, as a practical matter, we have some reassurance that variance based minimizations with the hybrid method can achieve accurate excitation energies without stability concerns in this system when relying on state-specific quantum chemistry

to provide orbital shapes. We now turn to more rigorous stability testing, where VMC orbital optimization plays a large role.

3.3. Stability Tests

To gain more insight into cases where stability issues might arise, we consider a series of excited state optimizations with the LM and the hybrid method. Our focus is now mainly on whether these optimizations progress stably rather than whether they fully reach the minimum or the precise accuracy of the excitation energies that might be obtained from them. The differences in technical optimization choices between the stable and unstable outcomes we observe may assist the work of other VMC practitioners.

To construct an ansatz for this analysis, we consider a (6e,10o) active space in a cc-pVDZ basis set with BFD pseudopotentials.[69] This is the same basis, pseudopotential and active space for which stability issues were recently observed.[28] We use a 0.001 coefficient cutoff for a 4-state-average CASSCF to obtain a CI expansion of 1892 determinants for the lowest excited state of CN5 and add one- and two-body Jastrow factors. The lowest excited state is a ground state within its symmetry and could have been described with a single state CASSCF, but here we allow determinants of other symmetries (which had coefficient above 0.001 for other states in the state-average but have zero coefficients for the lowest excited state) within our ansatz. The presence of these unnecessary determinants increases the difficulty of the optimization due to the effect in Figure 1 and the use of state-averaging may enhance the amount of orbital optimization being asked of VMC. While this ansatz is not as closely tailored for the excited state as quantum chemistry might allow, it remains a reasonable initial guess that still requires nontrivial optimization at the VMC level.

In order to assess stability issues that may appear gradually, we run our optimizations for a considerably larger number of iterations than we otherwise would for typical excitation energy predictions, aiming for many hundreds of LM iterations. We also provide the LM (and its blocked variant within the hybrid method) with only 100,000 samples per iteration in order to make long optimizations more practical and somewhat favor the potential emergence of stability issues due to poorer stochastic estimates. For comparison, we note that for a molecule as large as CN5, our typical practices would provide a million samples per LM iteration, potentially more in cases with many ansatz parameters, and only optimize for somewhere in the range of 50 to 100 iterations. For the hybrid method, we use 30,000 samples per AD iteration, which is a typical amount, and use 17 macro-iterations (each containing 100 AD steps and 3 blocked LM steps), which is significantly longer than our usual range of 5 to 10.

We begin with a fixed value of $\omega = -41.475$ and minimize the objective function Ω in a staged approach, first optimizing the less difficult Jastrow and CI parameters and only turning on orbital optimization at the next stage. We choose to optimize all determinants from CASSCF alongside the initially unoptimized Jastrow for a total of 2030 variational parameters in our first stage of optimization. We mention that in practical calculations, this stage could be performed even more cautiously, such as by optimizing the Jastrow with only the 100 most important determinants and then adding the remainder in sets of a few hundred with zero initial coefficients, but optimizing them all at once from the start provides us with a more stringent stability test.

Three optimizer choices are considered: LM with fixed shifts, LM with adaptive

shifts, and the hybrid method. These various options' approaches to the issue of step size control are a key way of distinguishing them. In both varieties of the LM as well as the blocked LM steps within the hybrid method, a correlated sampling procedure is performed to allow the possibility of rejecting a proposed parameter update. However, the fixed shift version of the LM has no means of constraining its step size beyond what the chosen shift values ($c_I = 0.1$ and $c_S = 1$) provide while the adaptive version can move from those initial values and thus alter both the size and direction of the LM updates, as explained above in Section 2.2. The hybrid method incorporates the benefits of the adaptive shift scheme in its use of the blocked LM and the step sizes employed during its AD sections dynamically adjust with the objective function gradients according to RMSprop. Throughout the hybrid method optimizations in this section, we divide parameters into 5 blocks and employ 30 parameter directions per block along with 5 directions from AD in the second phase of all blocked LM iterations.

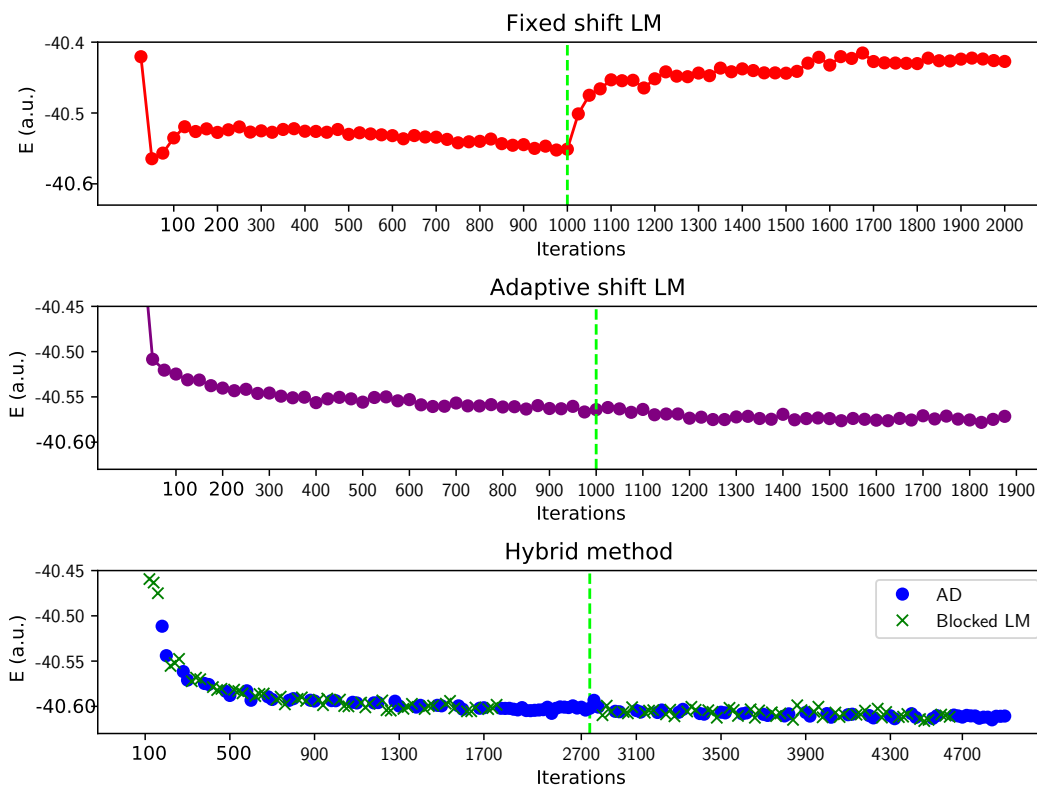


Figure 5. Excited state energy for fixed shift LM, adaptive shift LM, and hybrid method. Starting point was unoptimized Jastrow and CI coefficients from SA-CASSCF. Green dashed line marks the point at which orbital optimization is turned on.

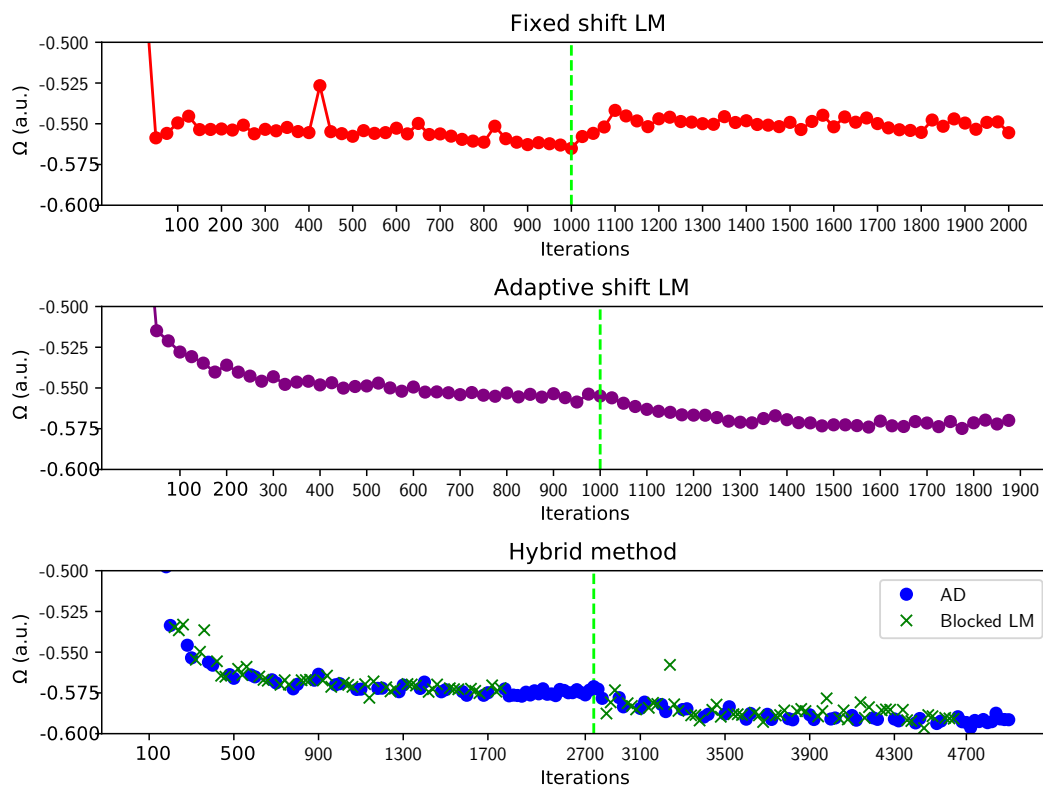


Figure 6. Objective function Ω for fixed shift LM, adaptive shift LM, and hybrid method. Starting point was unoptimized Jastrow and CI coefficients from SA-CASSCF. Green dashed line marks the point at which orbital optimization is turned on

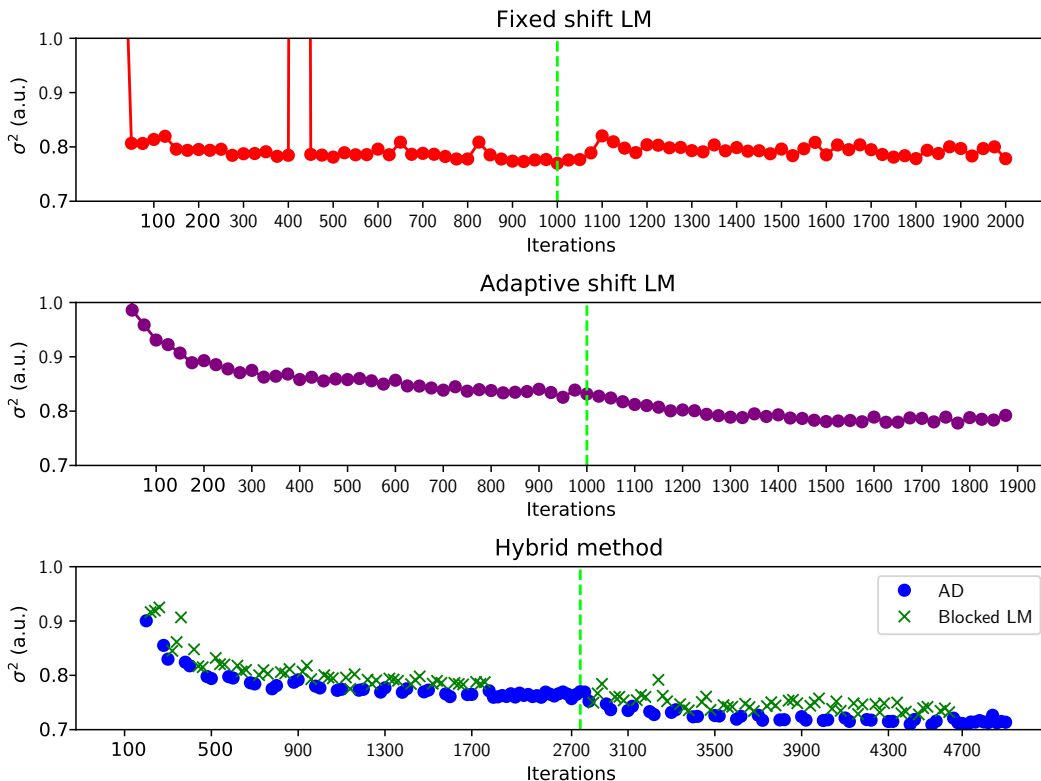


Figure 7. Excited state variance for fixed shift LM, adaptive shift LM, and hybrid method. Starting point was unoptimized Jastrow and CI coefficients from SA-CASSCF. Green dashed line marks the point at which orbital optimization is turned on. The separation between AD and blocked LM points is an artifact of autocorrelation.

Turning to the results, we consider the optimizations shown in Figures 5 through 7. Points on the LM plots represent the average of 25 LM iterations. On the hybrid method plots, dots are averages of 50 AD iterations and crosses are individual blocked LM iterations. The vertical scales have been chosen to make the varying stability behavior of the optimization algorithms more visible, which leaves off some points corresponding to early iterations. The vertical dashed line marks the end of the first stage of optimizing only Jastrow and CI parameters and the start of including orbital optimization. At the onset of orbital optimization, the initial values of the shifts were restored to $c_I = 0.1$ and $c_S = 1$ for the adaptive shift LM and the hybrid method, and the initial step sizes used in AD are changed. The initial hybrid method optimization of CI and Jastrow parameters used step sizes of 0.01 and 0.1 respectively. Once orbital optimization was turned on, these were reduced to 0.005 and orbital parameters were given a step size of 0.0001.

Focusing on the left-hand Jastrow and CI side of the three figures, we see that all approaches successfully lower the target function with the energy and variance also decreasing in tandem. The fixed shift LM case in the upper panel of the three figures provides some reason for concern with a sustained rise in the target function and energy within the first 100 iterations, but the optimization later recovers. The adaptive shift LM and the hybrid method provide smoother optimization, but for this case with only the easier Jastrow and CI parameters, their refinements for step size control may be less necessary.

We then turn on orbital optimization and continue to optimize the other parameters starting from each method’s Jastrow and CI result. We continue to keep ω fixed. With orbital optimization, our ansatz now has a total of 6163 variational parameters. We now see in the second half of Figures 5 through 7 that the three methods differ more dramatically. The fixed shift LM shows a substantial rise in energy of roughly 80 milli-Hartree over the course of hundreds of iterations. This failure of optimization is clearly signaled by a rise in the objective function in the first hundred iterations of orbital optimization. Both the energy and objective function remain elevated during hundreds of later iterations, indicating that the LM is unable to recover in this case. While the fixed shift LM in principle possesses the ability in the correlated sampling phase to detect and reject any step that would raise the objective function, this safeguard is clearly inadequate in this case. With poor estimates of the objective function at the current and proposed sets of ansatz parameters, the LM may mistakenly estimate that a step will lower the objective function only to discover otherwise once it is at the new point in parameter space and takes new samples. This danger is exacerbated if proposed parameter steps can remain incautiously large and uncertain, which fixing the LM shifts permits. Our finding of optimization failure with limited step control aligns with other observations of variance minimization instabilities when using a modified Newton method with a fixed, non-adaptive step damping parameter.[28]

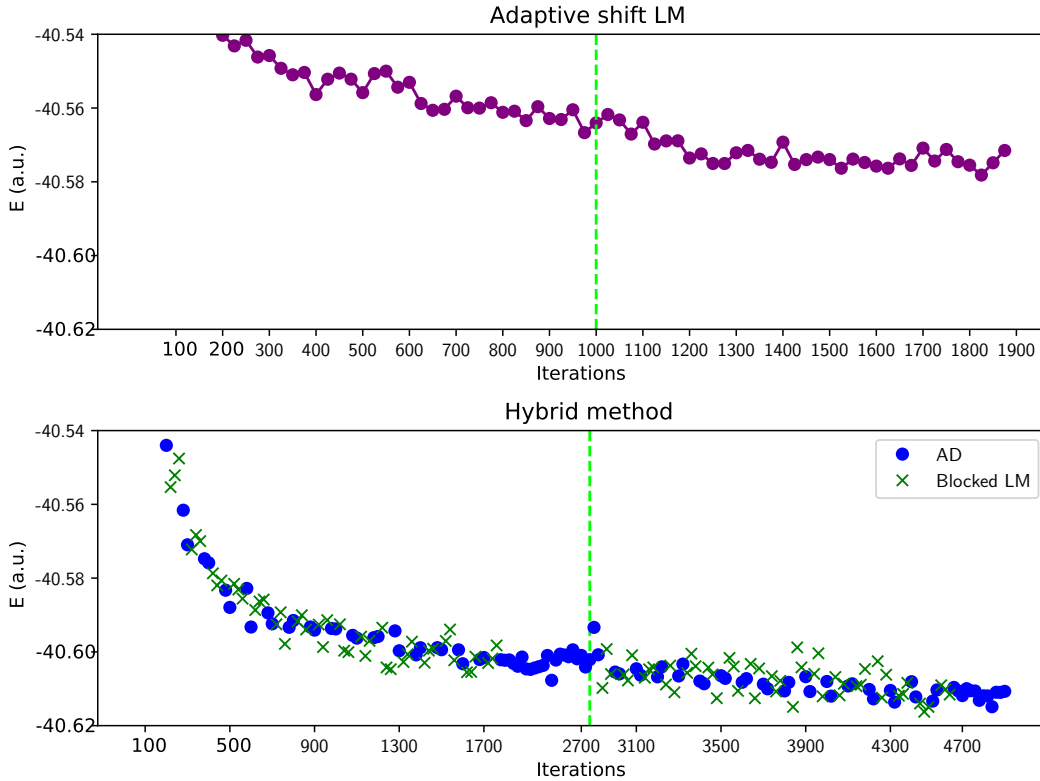


Figure 8. Zoomed in view of excited state energy for adaptive shift LM and hybrid method. Green dashed line marks the end of the first stage where only Jastrow and CI parameters are optimized.

The change from fixed to adaptive shifts yields far better performance for the LM, with steady decreases in objective function, energy, and variance. We provide a zoomed

in plot of the energy for the adaptive shift LM and hybrid method in Figure 8 to make clear that both approaches continue to lower the energy after enabling orbital optimization. The adaptive shift LM optimization makes only rather slow progress over many hundreds of iterations and after roughly 300 iterations with orbital optimization, the shifts are so large that only very minor changes are being made to the parameters in the remainder of the calculation. While this sluggish optimization would be undesirable in normal VMC applications, it clearly does not show any pathological behavior in terms of instability even though the adaptive shift LM is operating with only 100,000 samples per iteration. Although this low number of samples may hamper the LM's ability to determine effective parameter updates that would minimize more quickly, any stability challenges it might pose have been overcome with enhanced step control in the algorithm's design. Essentially, the adaptive shifts prevent the optimizer from pushing past the point where statistical uncertainty precludes effective update steps. The hybrid method is similarly stable and able to achieve significantly lower values of Ω , energy, and variance. The blocked LM iterations show some scatter in the objective function and the variance, but do not derail the stability of the optimization. The separation between the blocked LM and AD variance points in Figure 7, also seen in Figure 10, is an autocorrelation artifact from the low number of samples used to evaluate the AD variances being averaged together in each point and diminishes if AD iterations are given more samples (we do not do so as it is not necessary for effective optimization).

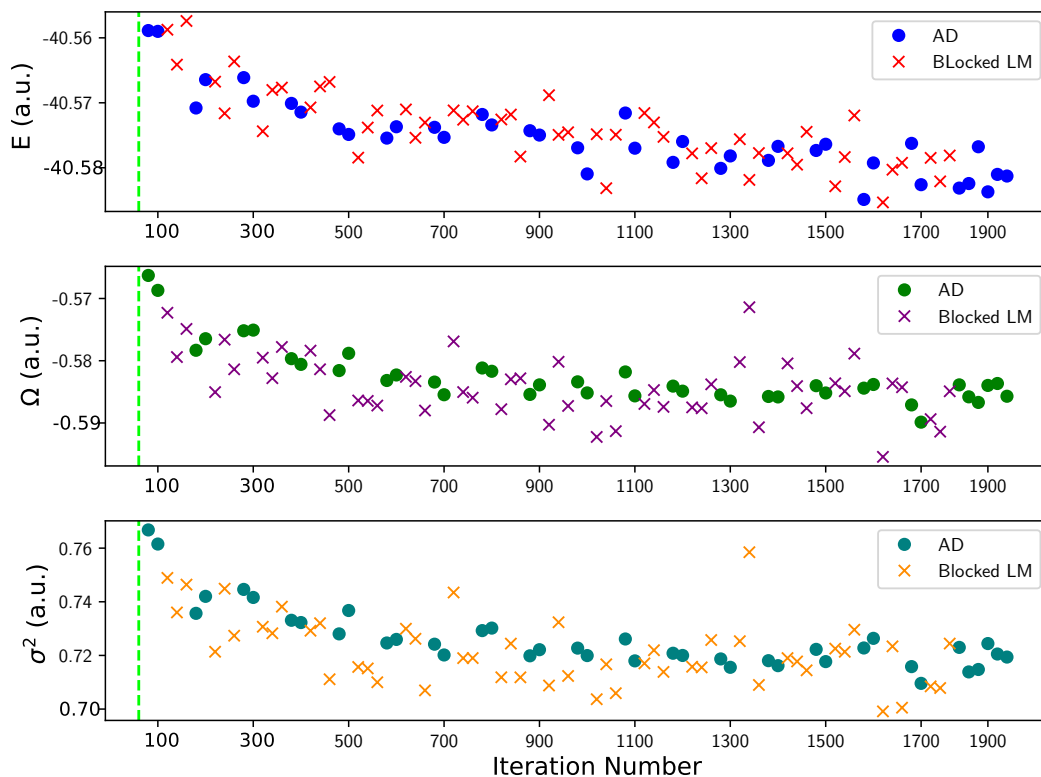


Figure 9. Optimization of all parameters including orbitals using the hybrid method starting from the end of the LM fixed shift optimization of only the Jastrow and CI parameters. Green line is shown to the left to make clear these plots show only the stage with orbital optimization.

We also consider the potential effects of the optimized MSJ starting point on the second, orbital optimizing, stage of the optimization. As depicted earlier in Figure 6, the hybrid method achieves a lower value of Ω than the two types of the LM during the first Jastrow and CI phase of optimization and therefore has a better initial wave function when orbital optimization is turned on. To check whether this difference has any stability consequences, we also performed a hybrid method optimization of all parameters beginning from the optimized MSJ ansatz obtained by the fixed shift LM. As shown in Figure 9, the hybrid method is still able to stably optimize from this inferior starting point. While the quality of the initial wave function may still influence how fully the hybrid method is able to minimize Ω , a somewhat poorer starting point does not destabilize the hybrid algorithm.

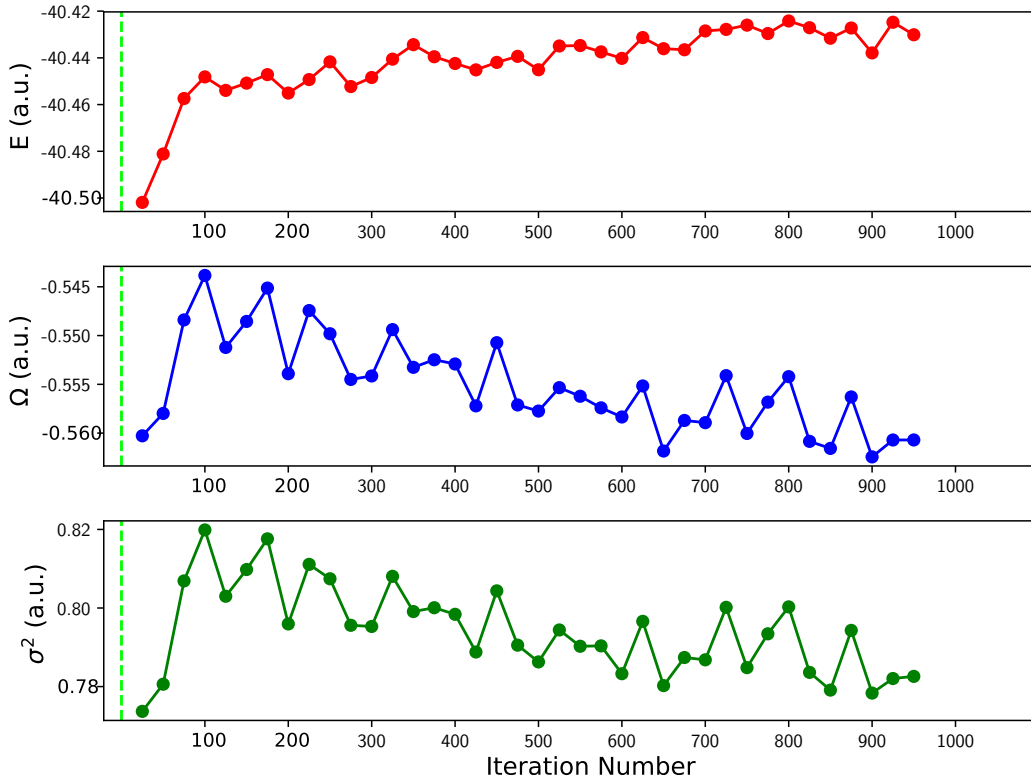


Figure 10. Optimization of all parameters including orbitals using the LM with fixed shifts while varying the energy targeting parameter ω on the fly. Starting point was the optimized MSJ wave function from the preceding LM fixed shift optimization of only the Jastrow and CI parameters. Green line is shown to the left to make clear these plots show only the stage with orbital optimization.

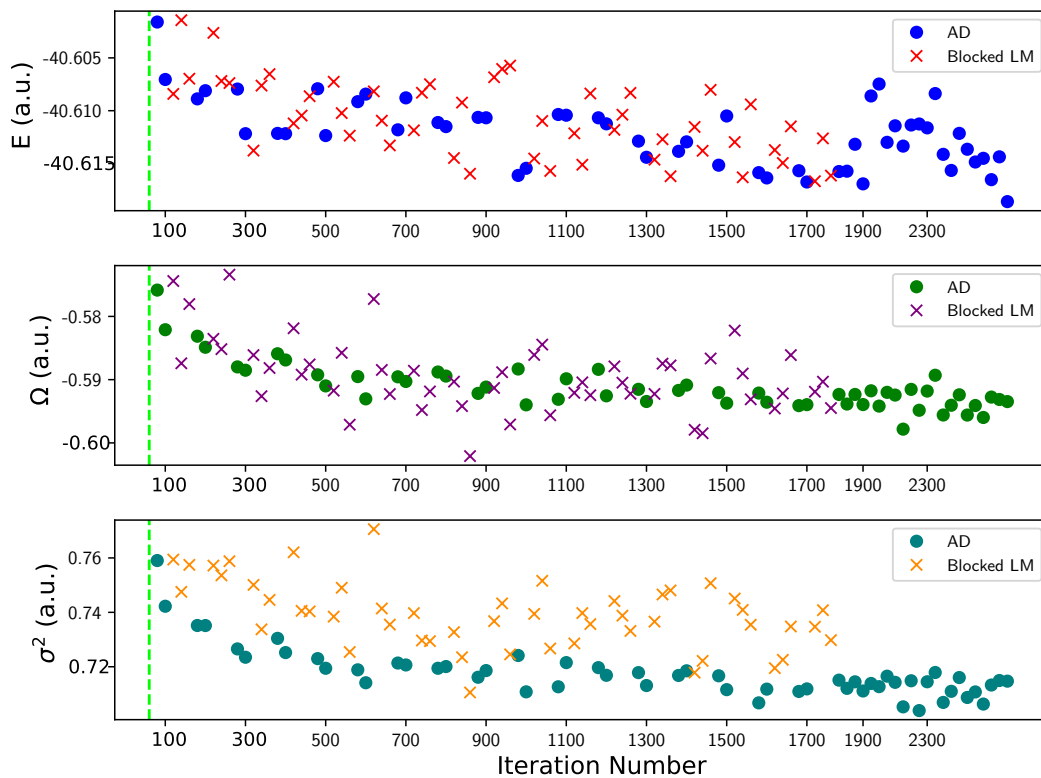


Figure 11. Optimization of all parameters including orbitals using the hybrid method while varying ω . Starting point was the optimized MSJ wave function from the preceding hybrid method optimization of only the Jastrow and CI parameters. Green line is shown to the left to make clear these plots show only the stage with orbital optimization. The separation between AD and blocked LM variance points is an artifact of autocorrelation.

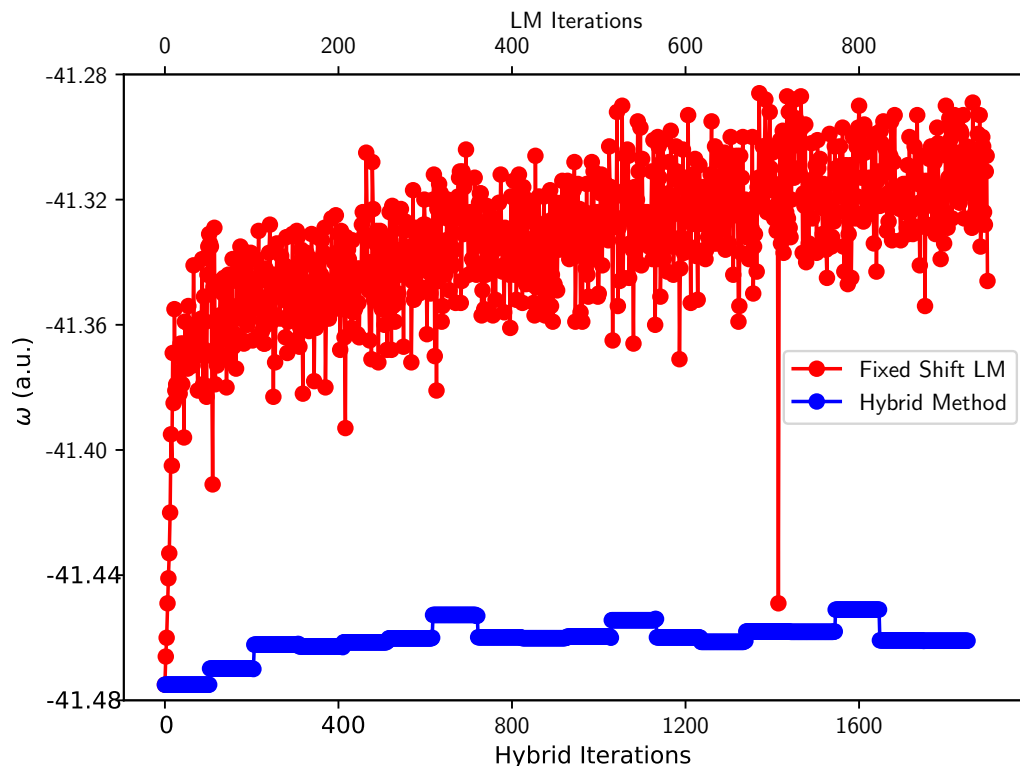


Figure 12. Varying values of omega over individual iterations during fixed shift LM and hybrid method optimizations of all parameters. The last 1000 iterations of AD in the hybrid optimization used the final value of omega on the last hybrid macro-iteration and are omitted from this plot.

The optimizations shown so far have all used a fixed value of ω . While in practical calculations, a series of fixed ω calculations is always an option for moving ω to transform minimization of Ω into variance minimization, for completeness we also consider varying ω over the course of a single optimization. For the fixed shift LM and the hybrid method, we again turn on orbital optimization at their respective optimized Jastrow and CI starting points, now with schemes for varying ω . For the LM, during the first 10 iterations, we interpolate^[31] ω between its initial value and $E - \sigma$, and afterward allow ω to float at the value of $E - \sigma$ set by the preceding iteration. For the hybrid method, we use the last 30 AD iterations in each macro-iteration to compute $E - \sigma$ for setting a new value of ω for the blocked LM steps and the AD section of the next macro-iteration. As seen in Figures 10 and 11, there is little difference in the methods' stability behavior from the fixed ω case. The fixed shift LM again shows a clear rise in the energy and variance while the hybrid method still performs a stable minimization. In Figure 10, the objective function Ω and the variance mostly recover while the energy does not, suggesting the lack of adaptive step control may be allowing the LM optimization to move into another basin of convergence. As Figure 12 shows, the value of ω is dragged up significantly during the unstable fixed shift LM optimization, while it only moves a little during the hybrid method. The hybrid method's stability suggests that varying ω and thus changing the objective function landscape on the fly are not the key factors in determining stability. Instead, we see again that the presence or absence of adaptive step control makes the difference.

4. Conclusions

The sequences of optimizations we have performed point to several considerations when seeking to ensure stable and successful applications of variance-based state-specific VMC. Scenarios characterized by large numbers of difficult parameters, as in orbital optimization, pose a significant risk of optimization instability from poor parameter updates. This difficulty is exacerbated if the amount of sampling is insufficient to overcome uncertainty coupling in the matrix diagonalization of large parameter sets or to be able to recognize and reject bad updates. Our findings on stability failures of the LM add to other observations of challenges in variance minimization[28] and help clarify when such optimization difficulties are most likely to be encountered. The nature of the optimization failures we encounter point to choices in optimizer design as the driver of variance minimization instabilities and do not offer any indication that shape of the variance surface is pathological. While the problem of optimization instability will remain a concern as researchers pursue studies of larger systems and more complex ansatzes, multiple tools are available for curbing its impact.

First, the ability to adaptively control step size and direction is a key element of robustness in challenging optimizations. Previously reported instabilities were seen in a setting that lacked adaptive step control, as were all the unstable runs in the present study. In contrast, optimizations in which we employ adaptive step control (either in the LM alone or in the hybrid method) proved stable. Second, algorithms can be designed to reduce the optimization burden on the portions most prone to instability. This idea is reflected in the hybrid method’s structure, with a large portion of the optimization left to the more stable AD and the reduction of the size of the LM matrices by first including only parameters of significant gradients and then blocking. Finally, careful construction of wave functions to effectively describe correlation while remaining readily optimizable at the VMC level is advantageous. We have shown that determining orbital shapes with state-specific quantum chemistry and optimizing only Jastrow and CI parameters is sufficient for an accurate excitation energy in CN5 and demonstrated the same idea for a broader set of molecules in recent work.[35] Circumventing VMC orbital optimization in this way avoids any stability challenges it might pose and greatly enhances computational efficiency. Taken together, these approaches provide reassurance that state-specific variance-based VMC can be performed in a robust and stable manner so long as adaptive step control is employed.

5. Acknowledgements

This work was supported by the Office of Science, Office of Basic Energy Sciences, the U.S. Department of Energy, Contract No. DE-AC02-05CH11231. Computational work was performed with the Berkeley Research Computing Savio cluster and the LBNL Lawrence cluster.

6. Disclosure Statement

No potential conflict of interest was reported by the authors.

7. Appendix

Table 2. Structure of CN5. Coordinates in Å.

C	0.000 000	0.000 000	0.340 620
C	0.000 000	1.188 120	-0.363 814
C	0.000 000	-1.188 120	-0.363 814
H	0.000 000	0.000 000	1.424 530
H	0.000 000	1.160 200	-1.449 150
H	0.000 000	-1.160 200	-1.449 150
N	0.000 000	2.389 120	0.164 413
N	0.000 000	-2.389 120	0.164 413
H	0.000 000	2.531 430	1.161 940
H	0.000 000	-2.531 430	1.161 940
H	0.000 000	3.211 380	-0.414 923
H	0.000 000	-3.211 380	-0.414 923

References

- [1] M.P. Nightingale and V. Melik-Alaverdian, *Phys. Rev. Lett.* **87** (4), 43401 (2001).
- [2] M. Casalegno, M. Mella and A.M. Rappe, *The Journal of Chemical Physics* **118** (16), 7193–7201 (2003).
- [3] C.J. Umrigar and C. Filippi, *Phys. Rev. Lett.* **94**, 150201 (2005).
- [4] S. Sorella, *Phys. Rev. B* **64**, 024512 (2001).
- [5] S. Sorella, *Phys. Rev. B* **71**, 241103 (2005).
- [6] J. Toulouse and C.J. Umrigar, *The Journal of Chemical Physics* **126** (8), 084102 (2007).
- [7] C.J. Umrigar, J. Toulouse, C. Filippi, S. Sorella and R.G. Hennig, *Phys. Rev. Lett.* **98** (11), 110201 (2007).
- [8] S. Sorella, M. Casula and D. Rocca, *J. Chem. Phys.* **127** (1), 014105 (2007).
- [9] E. Neuscamman, C.J. Umrigar and G.K.L. Chan, *Phys. Rev. B* **85** (4), 045103 (2012).
- [10] L.R. Schwarz, A. Alavi and G.H. Booth, *Phys. Rev. Lett.* **118** (17), 176403 (2017).
- [11] I. Sabzevari and S. Sharma, *J. Chem. Theory Comput.* **14** (2018).
- [12] D. Luo and B.K. Clark, *Phys. Rev. Lett.* **122**, 226401 (2019).
- [13] A. Mahajan and S. Sharma, *J. Phys. Chem. A* **123** (17), 3911–3921 (2019).
- [14] I. Sabzevari, A. Mahajan and S. Sharma, *The Journal of Chemical Physics* **152** (2), 024111 (2020).
- [15] L. Otis and E. Neuscamman, *Phys. Chem. Chem. Phys.* **21**, 14491–14510 (2019).
- [16] C.J. Umrigar, K.G. Wilson and J.W. Wilkins, *Phys. Rev. Lett.* **60**, 1719–1722 (1988).
- [17] P.R.C. Kent, R.J. Needs and G. Rajagopal, *Phys. Rev. B* **59** (19), 12344 (1999).
- [18] X. Lin, H. Zhang and A.M. Rappe, *J. Chem. Phys.* **112** (6), 2650–2654 (2000).
- [19] W.M.C. Foulkes, L. Mitas, R.J. Needs and G. Rajagopal, *Rev. Mod. Phys.* **73** (1), 33–83 (2001).
- [20] H. Huang and Z. Cao, *The Journal of Chemical Physics* **104** (1), 200–205 (1996).
- [21] H. Huang, Q. Xie, Z. Cao, Z. Li, Z. Yue and L. Ming, *The Journal of Chemical Physics* **110** (8), 3703–3707 (1999).
- [22] M.W. Lee, M. Mella and A.M. Rappe, *The Journal of Chemical Physics* **122** (24), 244103 (2005).
- [23] F. Cordova, L.J. Doriol, A. Ipatov, M.E. Casida, C. Filippi and A. Vela, *J. Chem. Phys.* **127** (16), 164111 (2007).
- [24] C. Filippi, M. Zaccheddu and F. Buda, *J. Chem. Theory Comput.* **5** (8), 2074–2087 (2009).
- [25] R. Send, O. Valsson and C. Filippi, *Journal of Chemical Theory and Computation* **7** (2), 444–455 (2011), PMID: 26596164.

- [26] R. Guareschi and C. Filippi, *Journal of Chemical Theory and Computation* **9** (12), 5513–5525 (2013), PMID: 26592286.
- [27] R. Guareschi, H. Zulfikri, C. Daday, F.M. Floris, C. Amovilli, B. Mennucci and C. Filippi, *J. Chem. Theory Comput.* **12** (4), 1674–1683 (2016).
- [28] A. Cuzzocrea, A. Scemama, W.J. Briels, S. Moroni and C. Filippi, *J. Chem. Theory Comput.* **16** (7), 4203–4212 (2020), PMID: 32419451.
- [29] M. Dash, S. Moroni, C. Filippi and A. Scemama, *Journal of Chemical Theory and Computation* **17** (6), 3426–3434 (2021), PMID: 34029098.
- [30] L. Zhao and E. Neuscamman, *J. Chem. Theory Comput.* **12**, 3436–3440 (2016).
- [31] J.A.R. Shea and E. Neuscamman, *J. Chem. Theory Comput.* **13** (12), 6078–6088 (2017), PMID: 29140699.
- [32] S.D.P. Flores and E. Neuscamman, *J. Phys. Chem. A* **123** (8), 1487–1497 (2019).
- [33] S.M. Garner and E. Neuscamman, *The Journal of Chemical Physics* **153** (14), 144108 (2020).
- [34] L. Otis, I. Craig and E. Neuscamman, *The Journal of Chemical Physics* **153** (23), 234105 (2020).
- [35] L. Otis and E. Neuscamman, arXiv preprint arXiv:2111.07221 (2021).
- [36] A. Domingo, M.À. Carvajal, C. de Graaf, K. Sivalingam, F. Neese and C. Angeli, *Theoretical Chemistry Accounts* **131** (9), 1264 (2012).
- [37] B. Meyer, A. Domingo, T. Krah and V. Robert, *Dalton Trans.* **43**, 11209–11215 (2014).
- [38] L.N. Tran, J.A.R. Shea and E. Neuscamman, *J. Chem. Theory Comput.* **15** (9), 4790–4803 (2019), PMID: 31393725.
- [39] A.K. Dutta, M. Nooijen, F. Neese and R. Izsák, *Journal of Chemical Theory and Computation* **14** (1), 72–91 (2018), PMID: 29206453.
- [40] B. Kozma, A. Tajti, B. Demoulin, R. Izsák, M. Nooijen and P.G. Szalay, *Journal of Chemical Theory and Computation* **16** (7), 4213–4225 (2020), PMID: 32502351.
- [41] P.F. Loos, M. Comin, X. Blase and D. Jacquemin, *Journal of Chemical Theory and Computation* **17** (6), 3666–3686 (2021), PMID: 33955742.
- [42] M. Dash, S. Moroni, A. Scemama and C. Filippi, *Journal of Chemical Theory and Computation* **14** (8), 4176–4182 (2018), PMID: 29953810.
- [43] M. Dash, J. Feldt, S. Moroni, A. Scemama and C. Filippi, *Journal of Chemical Theory and Computation* **15** (9), 4896–4906 (2019), PMID: 31348645.
- [44] L. Zhao and E. Neuscamman, *J. Chem. Theory Comput.* **13**, 2604–2611 (2017).
- [45] P.J. Robinson, S.D. Pineda Flores and E. Neuscamman, *J. Chem. Phys.* **147** (16), 164114 (2017).
- [46] F. Schautz and C. Filippi, *The Journal of Chemical Physics* **120** (23), 10931–10941 (2004).
- [47] J.R. Trail, *Phys. Rev. E* **77**, 016703 (2008).
- [48] J.R. Trail, *Phys. Rev. E* **77**, 016704 (2008).
- [49] R. Assaraf and M. Caffarel, *Phys. Rev. Lett.* **83** (23), 4682–4685 (1999).
- [50] C. Attaccalite and S. Sorella, *Phys. Rev. Lett.* **100**, 114501 (2008).
- [51] R. Assaraf and M. Caffarel, *The Journal of Chemical Physics* **113** (10), 4028–4034 (2000).
- [52] R. Assaraf and M. Caffarel, *The Journal of Chemical Physics* **119** (20), 10536–10552 (2003).
- [53] S. Pathak and L.K. Wagner, *AIP Advances* **10** (8), 085213 (2020).
- [54] J. van Rhijn, C. Filippi, S. De Palo and S. Moroni, *Journal of Chemical Theory and Computation* **18** (1), 118–123 (2022), PMID: 34930005.
- [55] J. Toulouse and C.J. Umrigar, *The Journal of Chemical Physics* **128** (17), 174101 (2008).
- [56] J. Kim, A. Baczewski, T.D. Beaudet, A. Benali, M.C. Bennett, M.A. Berrill, N.S. Blunt, E.J.L. Borda, M. Casula, D.M. Ceperley, B.K. Clark, R.C.C. Iii, K.T. Delaney, M. Dewing, K.P. Esler, H. Hao, O. Heinonen, P.R.C. Kent, J.T. Krogel, I. Kylänpää, Y.W. Li, M.G. Lopez, Y. Luo, F.D. Malone, R.M. Martin, A. Mathuriya, J. Mcminis, C.A. Melton, L. Mitas, M.A. Morales, E. Neuscamman, W.D. Parker, S.D.P. Flores, N.A. Romero, B.M. Rubenstein, J.A.R. Shea, H. Shin, L. Shulenburg, A. Tillack, J.P. Townsend, N.M. Tubman, B. Van Der Goetz, J.E. Vincent, D.C. Yang, Y. Yang, S. Zhang and L. Zhao,

- J. Phys. Condens. Matter **30** (19), 195901 (2018).
- [57] C. Filippi, R. Assaraf and S. Moroni, J. Chem. Phys. **144** (19), 194105 (2016).
- [58] R. Assaraf, S. Moroni and C. Filippi, J. Chem. Theory Comput. **13** (11), 5273–5281 (2017).
- [59] L.N. Tran and E. Neuscamman, J. Phys. Chem. A **124**, 8273–8279 (2020).
- [60] R. Hanscam and E. Neuscamman, arXiv **2111.02590** (2021).
- [61] P.R.C. Kent, A. Annaberdiyev, A. Benali, M.C. Bennett, E.J. Landinez Borda, P. Doak, H. Hao, K.D. Jordan, J.T. Krogel, I. Kylänpää, J. Lee, Y. Luo, F.D. Malone, C.A. Melton, L. Mitas, M.A. Morales, E. Neuscamman, F.A. Reboredo, B. Rubenstein, K. Saritas, S. Upadhyay, G. Wang, S. Zhang and L. Zhao, J. Chem. Phys. **152** (17), 174105 (2020).
- [62] P. Boulanger, D. Jacquemin, I. Duchemin and X. Blase, Journal of Chemical Theory and Computation **10** (3), 1212–1218 (2014), PMID: 26580191.
- [63] H.J. Werner, P.J. Knowles, F.R. Manby, J.A. Black, K. Doll, A. Heßelmann, D. Kats, A. Köhn, T. Korona, D.A. Kreplin, Q. Ma, T.F. Miller, A. Mitrushchenkov, K.A. Peterson, I. Polyak, G. Rauhut and M. Sibae, The Journal of Chemical Physics **152** (14), 144107 (2020).
- [64] Q. Sun, T.C. Berkelbach, N.S. Blunt, G.H. Booth, S. Guo, Z. Li, J. Liu, J.D. McClain, E.R. Sayfutyarova, S. Sharma, S. Wouters and G.K.L. Chan, WIREs Computational Molecular Science **8** (1), e1340 (2018).
- [65] A.A. Holmes, N.M. Tubman and C.J. Umrigar, J. Chem. Theory Comput. **12** (8), 3674–3680 (2016).
- [66] S. Sharma, A.A. Holmes, G. Jeanmairet, A. Alavi and C.J. Umrigar, J. Chem. Theory Comput. **13** (4), 1595–1604 (2017).
- [67] M.C. Bennett, C.A. Melton, A. Annaberdiyev, G. Wang, L. Shulenburger and L. Mitas, J. Chem. Phys. **147** (22), 224106 (2017).
- [68] Y. Garniron, A. Scemama, E. Giner, M. Caffarel and P.F. Loos, The Journal of Chemical Physics **149** (6), 064103 (2018).
- [69] M. Burkatzki, C. Filippi and M. Dolg, J. Chem. Phys. **126** (23), 234105 (2007).